

The Ground state of BiFeO₃: Low temperature magnetic phase transitions revisited

Arun Kumar and Dhananjai Pandey^{a)}

School of Materials Science and Technology, Indian Institute of Technology (Banaras Hindu University), Varanasi-221005, India.

ABSTRACT

Recent neutron diffraction and NMR studies suggest that the incommensurately modulated spin cycloid structure of BiFeO₃ is stable down to 4.2 K, whereas DC [M(T)] and AC [$\chi(\omega, T)$] magnetization, and caloric studies have revealed several magnetic transitions including a spin glass transition around 25 K. The two sets of observations are irreconcilable and to settle this, it is important to first verify if the low temperature magnetic transitions are intrinsic to BiFeO₃ or some of them are offshoots of oxygen vacancies and the associated redox reaction involving conversion of Fe³⁺ to Fe²⁺. We present here the results of M(T) and $\chi(\omega, T)$ measurements on pure and 0.3 wt% MnO₂ doped BiFeO₃ samples in the 2 to 300 K temperature range. It is shown that MnO₂ doping increases the resistivity of the samples by three orders of magnitude as a result of reduced oxygen vacancy concentration. A comparative study of the M(T) and AC $\chi(\omega, T)$ results on two types of samples reveals that the transitions around 25 K, 110 K and 250 K may be intrinsic to BiFeO₃. The widely reported transition at 50 K is argued to be defect induced, as it is absent in the doped samples. We also show that the spin glass transition temperature T_{SG} is less than the spin glass freezing temperature (T_f), as expected for both canonical and cluster glasses, in marked contrast to an earlier report of T_{SG} > T_f which is unphysical. We have also observed a cusp corresponding to the spin glass freezing at T_f in ZFC M(T) data not observed so far by previous workers. We argue that the ground state of BiFeO₃ consists of the coexistence of the spin glass phase with the long range ordered AFM phase with a cycloidal spin structure.

I. INTRODUCTION

Bismuth ferrite (BiFeO_3) is one of the most investigated magneto-electric multiferroics because of its room temperature multiferroicity with potential for applications in multifunctional devices of technological importance.¹⁻⁶ The room temperature ferroelectric phase of bulk BiFeO_3 corresponds to a rhombohedrally distorted perovskite structure in the $R3c$ space group⁷ in which the cations are displaced with respect to the anions along the [111] direction while the neighbouring oxygen octahedra are rotated in opposite directions (antiphase tilted structure in the $a^-a^-a^-$ tilt system⁸) about the same direction. The ferroelectric phase transition temperature is reported to be $T_C \sim 1103\text{K}$.⁹ The magnetic structure of BiFeO_3 corresponds to a non-collinear G -type antiferromagnetic ordering with a superimposed incommensurate magnetic modulation below the Neel temperature $T_N \sim 643\text{K}$.¹⁰ While the nuclear and magnetic structures as well as the multiferroic properties of BiFeO_3 at and above the room temperature are well settled⁴, there exists considerable controversy about its true ground state. Recent NMR studies suggest that the cycloidal modulation function for the magnetic phase changes from harmonic (sinusoidal) to anharmonic ($\text{sn}(x, m)$, elliptic Jacobi function) with m , which is a measure of anharmonicity, increasing from 0.48 at room temperature to 0.95 at 4.2 K¹¹⁻¹⁴. The neutron diffraction studies, which probe the space and time averaged magnetic structure at the bulk level, have also confirmed anharmonic nature of modulation of the cycloid at low temperatures^{15,16} but the anharmonicity is found to be much less, 0.50¹⁵ and <0.25 ¹⁶ in two independent studies using single crystals and polycrystalline samples, respectively, than that reported using a local probe like NMR. However, it is hard to imagine that the spin cycloid involving all the spins in the magnetic structure of BiFeO_3 will remain unaffected despite the several low temperature phase transitions that have been reported using a variety of measurement probes like DC magnetic susceptibility (χ_{DC}),¹⁷⁻²² AC magnetic susceptibility [$\chi'_{AC}(\omega, T)$ and $\chi''_{AC}(\omega, T)$],^{17,23} differential scanning calorimetry (DSC)^{18/}

differential thermal analysis (DTA),²⁴ Raman scattering²⁵⁻³¹ and elastic modulus spectroscopy.^{24,31} Towards understanding the true ground state of BiFeO₃, it is therefore important to settle if the low temperature phase transitions reported below room temperature are intrinsic to BiFeO₃ or some of them could be induced due to the presence of ionic vacancies created during high temperature processing. The present work was undertaken to address this issue.

Before presenting our results, we first briefly review the present status of the understanding of the low temperature phase transitions in BiFeO₃ and associated controversies. Historically, a frequency dependent anomaly in the temperature dependence of AC magnetic susceptibility well below the room temperature was first reported by Nakamura et al.²³ using splat quenched amorphous BiFeO₃ samples. Their results showed a cusp in $\chi'_{AC}(\omega, T)$ around $T_f \sim 21$ K with a spin glass transition temperature $T_{VF} \sim 14$ K. Splat quenching was used to suppress the Fe³⁺ to Fe²⁺ redox reaction, supposedly without affecting the magnetic ordering behaviour of BiFeO₃, which occurs due to the electrons released by the creation of oxygen vacancies in polycrystalline BiFeO₃ samples synthesized and sintered at high temperatures. Recent $\chi_{AC}(\omega, T)$ measurements on single crystals of BiFeO₃ have also revealed frequency dependent cusps around $T_f \sim 25$ K¹⁷ similar to that reported by Nakamura et al. though with a slightly higher cusp temperature that may possibly be due to crystalline nature of these samples. However, the spin glass transition temperature T_{SG} , which represents the critical slowing down of the spin dynamics, is reported to be ~ 29.4 K.¹⁷ The T_{SG} in the canonical and cluster spin glasses is known to be lower than the cusp temperature (T_f) corresponding to the lowest frequency of measurements and represents the divergence of the time scale associated with the slowest spin dynamics.³² Since the $T_{SG} \sim 29.4$ K reported by Singh et al. is greater than $T_f \sim 25$ K corresponding to the cusp temperature for their lowest frequency data (10 Hz), it calls for further investigation.

Besides the $\chi_{AC}(\omega, T)$ studies, several new low temperature magnetic transitions have been reported using zero field cooled (ZFC) and field cooled (FC) magnetization [$M(T)$] measurements in recent years.¹⁷⁻²² None of these measurements, however, reveal any anomaly around 21-25 K at which AC susceptibility studies reveal spin glass freezing. ZFC $M(T)$ measurements on polycrystalline powders of BiFeO_3 have revealed anomalies around 50 K,¹⁹ 150 K¹⁸ and 250 K.¹⁸ Further, the ZFC and FC $M(T)$ curves have been reported to bifurcate below 300 K but the anomaly around 50 K does not appear under the FC condition. This was taken as evidence for spin glass freezing (SG) or superparamagnetic (SPM) blocking. However, no corresponding anomaly is observed in $\chi'_{AC}(\omega, T)$ or $\chi''_{AC}(\omega, T)$ and therefore the possibility of this anomaly being linked with SG freezing or SPM blocking becomes remote. The anomaly around 50 K has also been reported in the ZFC $M(T)$ measurements on single crystals¹⁷ and nanocrystalline powders^{19,20} with a bifurcation temperature of ~ 250 K¹⁷ and just below 300 K,^{19,20} respectively. There are reports of anomalies around 65 K and 70 K as well but these have been subsequently found to be due to the presence of $\text{Bi}_2\text{Fe}_4\text{O}_9$ and $\gamma\text{-Fe}_2\text{O}_3$ impurity phases, respectively.^{21,22}

DSC measurements on polycrystalline BiFeO_3 have also revealed a strong specific heat anomaly at ~ 250 K similar to that observed in ZFC $M(T)$ data¹⁸ whereas the DTA analysis on BiFeO_3 single crystals suggests the possibility of a first order phase transition with a latent heat close to 150 K (~ 140 K).²⁴ Temperature dependence of the magnetic entropy, on the other hand, indicates five phase transitions occurring around 38 K, 150 K, 178 K, 223 K and 250 K.¹⁸ The dielectric measurements reveal weak anomalies around 55 K,²⁴ 140 K²⁴ and 215 K²⁴ for single crystals and around 25 K,²⁵ 50 K,²⁴ 200 K²⁴ and 220-260 K^{24,33} in ceramics. Elastic Modulus measurements reveal anomalies around 140 K^{24,31} and 200 K,²⁴ respectively. Further, Raman spectroscopic studies on polycrystalline and single crystals of BiFeO_3 have revealed transitions at 25 K,²⁵ 90 K,²⁷ 140 K,²⁶⁻³¹ 200 K²⁶⁻²⁸ and 250 K.²⁷ Taking into account the

observations made by different experimental probes discussed above, the transition occurring around 38-50 K, 140–150 K and 220–250 K have been attributed to magnetic but glassy with magnetoelectric coupling, predominantly magnetic transition involving spin reorientation, and antiferromagnetic (AFM) to spin glass (SG) transition with weak coupling with polarization, respectively.^{18, 24} The transition reported around 178 – 200 K has been proposed to be magnetoelastic in nature with a small coupling to polarization.²⁴

It is, however, quite intriguing to note that no single research group has reported all the low temperature transitions in the same sample. The fact that Nakamura et al. did not find any cusp in χ_{AC} around $T_f \sim 50$ K or signatures of other transitions above 50 K in splat quenched BiFeO₃ samples, supposed to be free from oxygen vacancies, also raises doubts about the intrinsic nature of various low temperature transitions other than the transition occurring around 25 K. Surprisingly, the low temperature M (T) measurements by various workers have not revealed the occurrence of the 25 K transition and its existence has been identified by χ_{AC} measurements,¹⁷ dielectric measurements²⁵ and Raman studies²⁵ only. To settle whether the various low temperature transitions reported by different workers are intrinsic to BiFeO₃ or some of them could be linked with cation/anion vacancies, we have carried out a comparative study of the low temperature phase transition behavior of polycrystalline BiFeO₃ samples with and without 0.3 wt% MnO₂ doping prepared under identical heat treatment conditions using DC magnetization [M (T)], and AC susceptibility [$\chi_{AC}(\omega, T)$] measurements. 0.3 wt% MnO₂ doped BiFeO₃ samples have been used to understand the role of oxygen vacancies since such a doping is known to decrease the oxygen vacancy concentration, enhance DC resistance of BiFeO₃ based ceramics and gives better quality P-E hysteresis loops.³⁴ Our results provide unambiguous evidence for spin glass freezing around $T_f \sim 25$ K in M (T) as well as $\chi_{AC}(\omega, T)$ in both the doped and undoped samples with a spin glass transition temperature $T_{SG} \sim 20$ K which, unlike the previous report,²³ is less than T_f , as expected for such glassy transitions. Our

results also suggest that the anomaly around 50 K could be due to extrinsic factors like oxygen vacancies as it is not present in the MnO_2 doped samples. The two other anomalies seen in the $M(T)$ of the doped sample seem to suggest that 250 K and 100-150 K transitions reported in the literature could also be intrinsic though it requires more investigation. Our results, in conjunction with the recent observations based on neutron and NMR studies, suggest that the ground state of BiFeO_3 corresponds to a coexistence of spin glass phase with the long range spin cycloid. We also discuss the implications of such a phase coexistence in terms of the existing theoretical models.

II. EXPERIMENTAL DETAILS

A. Sample Preparation: Both undoped and 0.3 wt% MnO_2 -doped BiFeO_3 powders were prepared by conventional solid state thermochemical reaction method using high purity oxides as starting materials: Bi_2O_3 (Aldrich, 99.9 %), Fe_2O_3 (Aldrich, 99 %) and MnO_2 (Alfa Aesar, 99.9%). We have added 0.3 wt% MnO_2 during calcination for the preparation of doped samples. The ingredient powders were taken in stoichiometric proportions and mixed in an agate mortar pestle for 3 hours and subsequently in a planetary ball mill using a zirconia jar and zirconia balls for 6 hours with acetone as the mixing media. After drying, the mixed powders were calcined at an optimized temperature of 1063 K for 8 hours in an open alumina crucible. The calcined powder was crushed and again ball milled for 4 hours. The powder was then mixed with 2 % poly vinyl alcohol (PVA) as a binder and pressed at a load of 70 KN into disks of 13mm diameter and about 1mm thickness in a hydraulic press using steel die. After binder burn-off at 773 K for 10 hours, sintering were carried out at 1073 K for 1 hour in closed alumina crucibles with calcined powder of the same composition as spacer powder for preventing the loss of Bi_2O_3 during sintering. The weight loss during sintering was less than 1%.

B. Characterizations: X-ray diffraction (XRD) measurements were carried out using an 18 kW copper rotating anode based (Rigaku, Japan) powder diffractometer operating in the Bragg-Brentano geometry fitted with a curved crystal monochromator in the diffraction beam. The data were collected in the 2θ range of 20 to 120 degrees at a step of 0.02 degrees. The XRD patterns were recorded from powders obtained after crushing the ceramic pellets and annealing the crushed powder at 773 K for 10 hrs for removal of stresses introduced during crushing. The DC resistivity of samples was measured using an electrometer (Keithley model no. 6517A). The dc magnetization measurements were carried out using a VSM (Quantum Design, PPMS) and MPMS SQUID (Quantum Design, MPMS-3) magnetometer in zero-field-cooled (ZFC) and field-cooled (FC) conditions from 2 K to 300 K using dc field of 500 Oe, 20000 Oe and 50000 Oe. For the ZFC measurements, the sample was first cooled from room temperature down to 2 K in the absence of a magnetic field. After applying the magnetic field at 2 K, the magnetization was measured in warming cycle. For the FC measurements, the sample was cooled from room temperature down to 2 K in the presence of magnetic field and magnetization was measured in warming cycle under the same field. The temperature dependent ac magnetic susceptibility measurements were carried out in an MPMS SQUID (Quantum Design MPMS-3) system using AC drive field of 5 Oe at various frequencies ranging from 97.3 Hz to 547.3 Hz. The chemical composition of the pure and 0.3wt% MnO_2 doped BiFeO_3 samples was checked by Energy Dispersive X-ray spectroscopic (EDX) technique using Carl-Zeiss Scanning Electron Microscope (SEM) model no. EVO 18. The composition was checked over individual grains and around grain boundaries separately. [Figs S1 and S2](#) of the [supplementary file](#) give the microstructure and the EDX spectra for the pure and 0.3wt% MnO_2 doped samples. The representative regions in the grain and at the grain boundaries are marked in the microstructures. The results of EDX analysis for the two types of samples are given in [Table S1](#). Similar analyses were carried out at five randomly selected regions and the average

composition is given in [Tables S2](#) for the pure and 0.3wt% MnO₂ doped samples. It is evident from these Tables that the average composition obtained by EDX analysis is close to the nominal (expected) composition within the standard deviation for Bi, Fe and Mn. The oxygen content for the pure sample is found to be a little less than that for the 0.3wt% MnO₂ doped sample. However, it is worth mentioning that EDX is not the ideal tool for the determination of oxygen content.

III. RESULTS AND ANALYSIS

A. Room Temperature Crystal Structure:

Single-phase powders and sintered ceramic samples of a BiFeO₃ are rather difficult to prepare because of the narrow temperature range of the stability of the perovskite phase³⁶⁻³⁸ and the volatile nature of Bi³⁺ that promotes the formation of impurity phases like Bi₂Fe₄O₉ and Bi₂₅FeO₃₉.^{37,38} [Fig.1.](#) shows the room-temperature x-ray powder diffraction (XRD) patterns of the undoped and 0.3 wt% MnO₂ doped BiFeO₃ powders. It is evident from the figure that both the samples are almost single phase as all the peaks correspond to the main perovskite phase of BiFeO₃ with only a trace amount of an impurity phase Bi₂Fe₄O₉ present with a peak intensity that is 1.4 % of the strongest 110 peak of BiFeO₃. It is evident from this figure that the 400_{pc} is a singlet while 222_{pc} and 440_{pc} are doublets with the weaker reflection occurring on the lower 2θ side, as expected for the stable rhombohedral phase in the R3c space group of BiFeO₃. This was further confirmed through Le-Bail profile fitting for the two samples (see [supplementary file](#) for more details). The refined lattice parameters and volume, as given in the [Table S3](#) of the [supplementary file](#), are in good agreement with those reported in the literature. The important inference is that the lattice parameters and volume are not affected by 0.3wt % MnO₂ doping.

B. DC Magnetization Studies:

Figs. 2. [(a), (b), and (c)], and Figs. 3. [(a), (b), and (c)] show the temperature dependent dc magnetization M (T) plots under ZFC and FC conditions for the undoped and doped samples for applied fields of 500, 20000 and 50000 Oe. The ZFC and FC magnetizations bifurcate well above 300K for the undoped samples whereas for the doped samples it begins around 270K at 500 Oe field. The irreversibility of the M (T) plots under ZFC and FC conditions increases with decreasing temperature suggesting spin-glass or superparamagnetic behavior in BiFeO_3 at low temperatures as proposed by previous workers also.^{17,23} The ZFC and FC magnetization curves of both the samples in the 300 to \sim 150 K range are consistent with conventional antiferromagnetic (AFM) behaviour in which magnetization is expected to decrease with decreasing temperature below T_N . However, both the samples show an upturn in magnetization below \sim 150K. This can happen as a precursor effect to impending phase transition(s) and accordingly a spin reorientation transition^{26,27,29} around 150-200K similar to that in orthoferrites,^{39,40} with the involvement of electromagnons,^{26,29} has been proposed.¹⁷ Such a spin reorientation transition has recently been reported in monoclinic compositions of solid solutions of BiFeO_3 with PbTiO_3 but the transition temperature is well above the room temperature and just below the T_N .⁴¹ In pure BiFeO_3 , the situation is quite different as spin reorientation has been proposed well below room temperature. However, the ZFC M (T) plot of undoped sample (Fig. 2) does not show any anomaly in the 150 to 200K range, other than the upturn in magnetization around 150K. The corresponding ZFC plot for the doped sample (Fig. 3), however, shows one weak cusp around 110 K. We believe that the presence of vacancy defects in the undoped samples masks this weak anomaly, even though there are indirect indications of such a transition in the undoped sample as well through the upturn in ZFC M (T) and observation of electromagnons.^{26,29} What is, however, more significant is the presence of two additional cusps occurring below 110 K, one around 50 K and another around 25 K, in the ZFC M [T] of the undoped sample, whereas the corresponding ZFC plot for the doped sample

shows only one prominent cusp around 25K. The cusp around 25K in ZFC $M(T)$ has not been observed in previous studies on single crystal¹⁷ and polycrystalline^{18,19} samples including the early work of Nakamura et al.²³ This clearly underlines the significance of quality and stoichiometry of the sample used in the present investigation in revealing such weak transitions below room temperature and a lack of this is probably the reason why no single worker has so far observed all the low temperature phase transitions in BiFeO_3 . The fact that the FC $M(T)$ does not show the 25K cusp in both the samples suggests that it could be due to spin glass freezing or superparamagnetic blocking or pinning of a magnetic impurity phase. Further, the absence of the cusp around 50 K in the doped samples suggests that it is a defect (vacancies) induced transition⁴²⁻⁴⁴ that gets suppressed due to MnO_2 doping as explained later in this paper. It is interesting to note that the 50 K cusp is observed for the undoped samples under both the ZFC and FC conditions for 500 Oe field suggesting that the spin dynamics associated with this defect-induced cusp is too fast to be frozen or blocked at 500 Oe. On increasing the field strength to 20000 Oe, the 50 K cusp becomes less prominent and it completely disappears in the 50000 Oe field measurement. This suggests that this transition could be associated with faster spin dynamics as compared to the 25K transition and requires higher field to freeze or block the spins. Below 10 K, both ZFC and FC curves show increase in the magnetization indicating a weak ferromagnetic behavior of BiFeO_3 at such low temperatures, as noted by previous workers also.^{17,18} Since the magnetization values (0.001emu/g) associated with the ferromagnetic rise of $M(T)$ are very small, it is most likely associated with some trace amount of impurities.⁴ The $M(T)$ plots of doped BiFeO_3 show an additional cusp, though very much less prominent as compared to that at T_f , around 260 K in the ZFC and FC conditions. This cusp is not seen in the corresponding plots for the undoped samples. Since doping is expected to suppress the oxygen vacancy concentration, as explained in more detail later on, we believe that the cusps around 25, 110 and 260 K observed in the ZFC $M(T)$ plot of the doped sample

are intrinsic to BiFeO₃. The previous workers, except Ref,¹⁸ did not observe the anomaly 260 K in the ZFC M (T) plots.^{17,19-22}

C. AC Susceptibility Studies:

In order to determine whether the cusps observed in the M (T) plots below 50 K are due to SG freezing or SPM blocking, we investigated the temperature dependence of the spin relaxation time τ from AC susceptibility ($\chi(\omega, T)$) measurements. The spin relaxation time τ is the dynamical fluctuation time scale corresponding to the measurement frequency at the peak temperature of the real part of AC magnetic susceptibility. The spin relaxation time (τ) for an assembly of non-interacting superparamagnetic particles slows down gradually as per the Arrhenius law:^{32,45}

$$\tau = \tau_0 \exp\left(\frac{E_a}{k_B T}\right) \quad (1)$$

where E_a is the anisotropy energy barrier equal to KV, where K is the anisotropy energy constant and V is the volume of the particles. In the spin glass systems, on the other hand, one observes critical slowing down of the spin dynamics at a characteristic spin glass transition temperature T_{SG} at which there is ergodicity breaking. In the canonical spin glass systems, an empirical Vogel-Fulcher (VF) law is used to model the critical slowing down of the spins:^{32,45}

$$\tau = \tau_0 \exp\left(\frac{E_a}{k_B (T - T_{VF})}\right) \quad (2)$$

where τ_0 is the time constant corresponding to the attempt frequency, k_B is the Boltzmann constant, E_a is the thermal activation energy and T_{VF} is the Vogel-Fulcher freezing temperature ($0 < T_{VF} < T_f$) like T_{SG} . In addition to VF law, a scaling law has also been proposed to characterize the SG transition. The scaling hypothesis assumes that the relaxation time (τ) is

related to the correlation length (ξ) near the SG transition temperature (T_{SG}). As ξ diverges at T_{SG} , relaxation time also diverges³² as:

$$\tau = \tau_0 \exp\left(\frac{T_f}{T_{SG}} - 1\right)^{-z\nu} \quad (3)$$

where τ_0 is the characteristic time scale for the spin dynamics, T_f is the maximum temperature corresponding to peak in the real part of $\chi'_{AC}(\omega, T)$, T_{SG} is the spin glass transition temperature in the limit of zero frequency, z is the dynamic scaling exponent, and ν is the critical exponent.

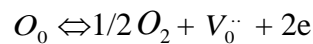
Fig. 4. and Fig. 5. show the real [$\chi'_{AC}(\omega, T)$] and imaginary [$\chi''_{AC}(\omega, T)$] parts of AC magnetic susceptibility measured with an applied ac drive field of 5 Oe in the frequency range 97.3 Hz to 547.3 Hz for undoped and doped BiFeO₃ respectively. It is evident from the figures that the peak temperatures corresponding to the real and imaginary parts of AC magnetic susceptibilities shift towards higher temperatures with increasing frequency which can be due to spin glass freezing or SPM blocking. For SPM blocking, $\ln \tau$ versus $1/T$ plot should be linear as per Eq. 1. The non-linear nature of the plots shown in Fig. 6. [(a), (b)] thus rules out SPM blocking in BiFeO₃ at low temperatures. Vogel-Fulcher law,³² on the other hand, provides excellent fit for both the undoped and doped samples, as can be seen from Fig. 6. [(a), (b)], confirming the spin glass freezing with a spin glass transition temperature $T_{SG} \sim T_{VF} \sim 20$ K. Attempts to fit the power law type behavior given by Eq. 3 gave inferior fits as shown in Fig. S4 [(a), (b)] of the [supplementary file](#). In fact, the power-law type critical dynamics misses the low frequency T_f data point and the best fit shown in the figures given in the supplementary file after excluding the low frequency data point is still inferior to that obtained by V-F law. The results of the best fit for V-F and power law behaviours are given in Table I. Interestingly, the value of the T_{SG} obtained by power law fit is very close to T_{VF} . Also, the exponent ($z\nu \sim 1.5 - 1.8$) is somewhat higher than that reported by Singh et al.¹⁷ for single crystal

BiFeO₃ and closer to the hydrodynamic model or mean field model for which $z\nu \sim 2$.⁴⁶ The activation energy E_{act} for the V-F law (0.8 meV or about 9.5 K) is comparable to the activation energies reported for the Eu_{1-x}Sr_xS system but lower than those for the canonical RKKY type spin glass systems. Our results thus confirm unambiguously that the anomaly observed around $T_f \sim 25$ K in BiFeO₃ is due to spin glass freezing with a spin glass transition temperature $T_{\text{SG}} \sim 20$ K at which the ergodicity is broken. Our results also show that the earlier report¹⁷ of $T_{\text{SG}} > T_f$ in BiFeO₃ is not correct and may be an artifact of numerical fit. By definition also, the T_{SG} cannot be higher than $T_f(\omega)$ as it corresponds to the value $T_f(\omega)$ in the limit of ω tending towards zero at which the slowest spin dynamics diverges.

IV. DISCUSSION OF RESULTS

A. Role of MnO₂ doping:

It is well known that the electrical and magnetic properties of pure BiFeO₃ are strongly influenced by oxygen vacancies created during sintering of BiFeO₃. Each oxygen vacancy leaves behind two electrons as per the following reaction written in the Kröger-Vink notation.⁴⁷



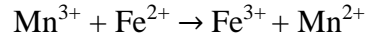
Electrons released due to oxygen vacancy may be captured by Fe³⁺ of BiFeO₃ leading to its reduction to Fe²⁺:



The presence of Fe²⁺ and Fe³⁺ ions leads to hopping of electrons due to which conductivity increases. Poor insulating resistance masks the observation of intrinsic ferroelectric polarization through the P-E hysteresis loop measurements and therefore such samples are not desirable for multiferroic applications. The Fe³⁺ to Fe²⁺ redox reaction also raises the possibility of creating local ferromagnetic clusters⁴⁸ via double exchange mechanism and may thus

enhance the magnetization.⁴⁹⁻⁵³ Theoretically, the role of intrinsic point defects, especially oxygen vacancies, as a possible source of magnetization in BiFeO₃⁵⁴ has been quite controversial. Ederer and Spaldin investigated the effect of oxygen vacancies on the weak ferromagnetism of BiFeO₃ using first principle calculations.⁵⁵ They found that oxygen vacancies lead to the formation of Fe²⁺ which can be identified by the clear qualitative differences in the local density of states, but the actual charge disproportionation is small. Paudel et al.⁵⁶ also studied the intrinsic defects in bulk BiFeO₃ and their effect on magnetization using first-principles approach. They found that the dominant defects in oxidizing (oxygen-rich) conditions are Bi and Fe vacancies and in reducing (oxygen-poor) conditions are O and Bi vacancies. The calculated carrier concentration shows that the BiFeO₃ grown in oxidizing conditions has p-type conductivity. The conductivity is reported to decrease with decreasing oxygen partial pressure, and the material shows insulating behaviour or n-type conductivity. According to these calculations, the Bi and Fe vacancies produce a magnetic moment of $\sim 1\mu_B$ and $5\mu_B$ per vacancy, respectively, for p-type BiFeO₃ and none for insulating BiFeO₃. O vacancies do not introduce any moment for both p-type and insulating BiFeO₃. Since our samples are sintered in close atmosphere, so there is a possibility that the BiFeO₃ becomes n-type due to oxygen vacancies. Mn-doping is known to reduce the dielectric losses, increase the dc resistivity and improve the magnetization behaviour of BiFeO₃.^{34,48-53} In case of our samples, the resistivity of undoped BiFeO₃ measured at room temperature is $1.6 \times 10^7 \Omega \text{ cm}$ while for the 0.3wt% MnO₂-doped BiFeO₃, the resistivity increases by three orders of magnitude to $1.09 \times 10^{10} \Omega \text{ cm}$ which is comparable to that reported by Kumar et al. in Mn substituted BiFeO₃.⁵³ In MnO₂ doped BiFeO₃ sample, the higher resistivity is expected due to donor doping of Mn and reduced oxygen vacancy concentration. Mn⁴⁺ ion plays a role of donor in BiFeO₃ because it possesses a higher valence than Fe³⁺. The addition of Mn⁴⁺ to BiFeO₃ requires charge compensation, which can be achieved by redox reaction involving capture of

electron by Mn^{4+} ion reducing it to Mn^{3+} . Further, the Mn ion is a multi-valence ion (Mn^{2+} , Mn^{3+} and Mn^{4+}) which can be oxidated or reduced during the sintering processes. However, it has been reported⁵³ that Mn^{4+} ion is not stable at high temperature and only Mn^{3+} and Mn^{2+} ions are stable in the ceramics at the sintering temperatures. Thus the following redox reaction can take place:⁵²



This reaction can effectively suppress the conversion of Fe^{3+} to Fe^{2+} and reduce the n-type doping effect due to oxygen vacancies leading to the observed increase in the resistivity of doped samples. According to the Shannon et al., the Mn^{3+} (ionic radius $r = 0.645 \text{ \AA}$) ion can occupy the Fe^{3+} ($r = 0.645 \text{ \AA}$) sites in BiFeO_3 materials, because both have the same valence state and ionic radius. So irrespective of the current level of understanding of the defect induced magnetism based on first principle calculations, MnO_2 doping does reduce the ionic vacancy concentrations and this may be responsible for the suppression of the 50 K cusp in the ZFC M (T) in the doped samples. Based on this discussion, we conclude that due to 0.3 wt% MnO_2 doping with reduced ionic vacancy concentrations, the intrinsic nature of the low temperature phase transitions in BiFeO_3 gets revealed unambiguously.

B. Anomalous AC Susceptibility Response of BiFeO_3 :

Having established the existence of spin glass freezing around 25K in BiFeO_3 as an intrinsic feature, we now turn to some intriguing aspects of AC $\chi(\omega, T)$. Firstly, the peak height of $\chi'(\omega, T)$ increases with increasing frequencies which is unusual as the susceptibility always decreases with increasing frequency except near frequencies corresponding to a resonant absorption that may be linked with the resistance, capacitance and inductance of the entire circuit rather than just the sample. In principle, it is possible to push the resonance frequencies to higher side by reducing the capacitance and inductance of the circuit by reducing the sample

quantity. However, this was not possible in BiFeO₃ due to very weak signal for the $\chi'(\omega, T)$. A similar anomalous AC magnetic susceptibility data has been reported in single crystal samples of BiFeO₃.¹⁷ It is also important to note that the imaginary part $\chi''(\omega, T)$ shows negative cusps at T_f with a peak temperature above the corresponding peak temperature for the real part $\chi'(\omega, T)$. The negative value clearly suggests that the circuit is no longer purely inductive except at very low temperatures ($< \sim 10\text{K}$). The third intriguing aspect of the $\chi''(\omega, T)$ is the presence of a tiny peak around 10K below which the imaginary part shows positive value. All these features require further study, as some of these anomalous features have also been tentatively attributed to the coexisting modulated magnetic structure of BiFeO₃,^{15,16,57-61} not observed in the conventional spin glass systems. Further, the occurrence of a spin glass phase in a homogeneously ordered system like BiFeO₃ without any quenched impurity and randomness requires further investigation as the existing models of spin glass transitions are based on the concept of disorder, randomness and frustration.³²

C. Ground State of BiFeO₃:

BiFeO₃ shows non-collinear AFM ordering with Heisenberg spins with an incommensurately modulated cycloidal spin structure superimposed on it. As said earlier, recent neutron scattering^{15,16,57-61} and NMR studies¹¹⁻¹⁴ suggest that this spin cycloid is stable down to the lowest temperature ($\sim 5\text{K}$). Considering these observations in conjunction with the present results, the most likely scenario for the ground state of BiFeO₃ is the coexistence of the spin glass phase and the long range ordered spin cycloid. The coexistence of LRO AFM and spin glass state has been a subject of extensive theoretical and experimental investigations for both Ising and Heisenberg systems.⁶²⁻⁶⁵ In some of the Heisenberg systems, it has been predicted theoretically⁶² and verified experimentally^{63,64} that the coexistence is due to the freezing of the transverse component of the spins.⁶⁵ An alternative proposal in disordered systems like PbFe_{0.5}Nb_{0.5}O₃ (PFN) whereby the two phases result from two different magnetic

sublattices, one (LRO) with percolative path ways and the other due to isolated Fe-O-Fe clusters, has also been proposed.⁶⁶ Pure BiFeO₃ has no quenched disorder per say, except for the possibility of Fe²⁺ ions in the magnetic sublattice replacing some of the Fe³⁺ sites due to redox reaction caused by oxygen vacancies and raising the possibility of local ferromagnetic interactions via double exchange. However, even though the oxygen vacancy concentrations, and hence the proportion of Fe²⁺ and Fe³⁺ in the magnetic sublattice, are expected to be significantly different in our undoped and doped BiFeO₃, the spin glass phase occurs below the same temperature T_f with similar spin glass transition temperatures T_{SG} and activation energies E_{act}. This indirectly suggests that the oxygen vacancies do not significantly influence the spin glass phase. In the absence of disorder in the magnetic sublattice or any frustrated interaction between the spins, the most likely possibility for the emergence of the spin glass phase is due to the freezing of the transverse component of the spins. Local magnetic probe like NMR¹¹⁻¹⁴ and the global probes like neutron scattering^{15,16} have revealed the possibility of distortions in the long range ordered magnetic modulated structure even though the extent of distortion from harmonic modulation is much less for the average structure, probed by the bulk techniques like neutron scattering, than that reported by local probe like NMR. Whether this anharmonicity is linked with the gradual transverse freezing of the spins or not needs further investigation using neutron scattering studies on single crystals.

V. CONCLUSIONS

The DC magnetization and AC susceptibility measurements on pure BiFeO₃ and 0.3 wt% MnO₂ doped BiFeO₃ show the existence of spin glass freezing around 25 K with a spin glass transition temperature T_{SG} ~20 K. The anomaly around 50 K could be due to extrinsic factors like oxygen vacancies as it is not present in the MnO₂ doped samples where the vacancy concentration is drastically reduced. The two other anomalies seen in the M (T) of the doped sample seem to suggest that 250 K and 100-150 K transitions are also intrinsic to BiFeO₃.

Combining the recent neutron and NMR studies on the presence of long range ordered magnetic phase at low temperatures (upto ~ 5K) and the present results, the most likely scenario for the ground state of BiFeO₃ is the coexistence of spin glass phase with the long range ordered spin cycloid with somewhat anharmonic modulation.

SUPPLEMENTARY MATERIALS

See [supplementary file](#): EDX analysis, LeBail profile fitting, refined unit cell parameters at room temperature and Power-law analysis for pure and 0.3 wt% MnO₂ doped BiFeO₃.

ACKNOWLEDGEMENTS

The authors thank Dr. Alok Banerjee, UGC-DAE Consortium for Scientific Research Indore, India for magnetization measurements. Dhananjai Pandey acknowledges financial support from Science and Engineering Research Board (SERB) of India through J. C. Bose Fellowship grant. The authors also acknowledge to Girish Sahu, CIF, IIT (BHU) Varanasi for EDX analysis.

References:

- ¹W. Eerenstein, N. D. Mathur, and J. F. Scott, *Nature (London)* **442**, 759 (2006).
- ²R. Ramesh, and N. A. Spaldin, *Nat. Mater.* **6**, 21(2007).
- ³S. -W. Cheong and M. Mostovoy, *Nat. Mater.* **6**, 13(2007).
- ⁴G. Catalan, J. F. Scott, *Adv. Mater.* **21**, 2463 (2009)
- ⁵M. Fiebig, *J. Phys. D* **38**, R123 (2005).
- ⁶J. H. Lee and R. S. Fishman, *Phys. Rev. Lett.* **115**, 207203 (2015).
- ⁷A. J. Jacobson and B. E. F. Fender, *J. Phys. C* **8**, 844 (1975).
- ⁸A. M. Glazer, *Acta Crystallogr. Sect. B: Struct. Crystallogr. Cryst. Chem.* **28**, 3384 (1972).
- ⁹W. Kaczmarek and Z. Pajak, *Solid State Commun.* **17**, 807 (1975).
- ¹⁰Y. E. Roginskaya, Tu. Ya. Tomashpolskii, Yu. N. Venevtsev, V. M. Petrov, and G. S. Zhdanov, *Sov. Phys. JETP* **23**, 47 (1966).
- ¹¹A. V. Zalesky, A. A. Frolov, T. A. Khimich, A. A. Bush, V. S. Pokatilov and A. K. Zvezdin, *Europhys. Lett.* **50** 547 (2000).
- ¹²A. V. Zaleskii, A. K. Zvezdin, A. A. Frolov and A. A. Bush, *JETP Lett.* **71** 465 (2000).
- ¹³D. F. Kozheev, A. V. Zalesky, A. A. Gippius, E. N. Morozova and A. A. Bush, *PhysicaB*, **329** 848 (2003).
- ¹⁴A. V. Zaleskii, A. A. Frolov, A.K. Zvezdin, A. A. Gippius, E. N. Morozova, D. F. Khozeev, A. S. Bush, V. S. Pokatilov, *JETP* **95**, 101 (2002).
- ¹⁵M. Ramazanoglu, W. Ratcliff II, Y. J. Choi, S. Lee, S.-W. Cheong, and V. Kiryukhin, *Phys. Rev.B* **83**, 174434 (2011).

- ¹⁶I. Sosnowska and R. Przeniosło, *Phys.Rev.B* **84**, 144404 (2011).
- ¹⁷M. K. Singh, W. Prellier, M. P. Singh, R. S. Katiyar and J.F. Scott, *Phys. Rev. B* **77**, 14440 (2008).
- ¹⁸B. Ramachandran and M.S. R. Rao, *Appl. Phys. Lett.* **95**, 142505 (2009).
- ¹⁹T. J. Park, G. C. Papaefthymiou, A. J. Viescas, A. R. Moodenbaugh and S. S. Wong, *Nano Lett.* **7**, 766-772 (2007).
- ²⁰S. Vijayanand, M. B. Mahajan, H.S. Potdar, and P.A. Joy, *Phys. Rev.B* **80**, 064423 (2009).
- ²¹R. Mazumdar, S. Ghosh, P. Mondal, D. Bhattacharya, S. Dasgupta, N. Das, A. Sen, A. K. Tyagi, M. Sivakumar, T. Takami, and H. Ikuta, *J. Appl. Phys.* **100**, 033908 (2006).
- ²²H. Naganuma, and S. Okamura, *J. Appl. Phys.* **101**, 09M103 (2007).
- ²³S. Nakamura, S. Soeya, N. Ikeda, and M. Tanaka, *J. Appl. Phys.* **74**, 5652 (1993).
- ²⁴S.T.A. Redfern, C. Wang, J.W. Hong, G. Catalan, and J.F. Scott, *J. Phys.: Condens. Matter* **20** 452205 (2008).
- ²⁵B. Ramachandran, A. Dixit, R. Naik, G. Lawes and M. S. R. Rao, *J. Appl. Phys.* **110**, 104105 (2011).
- ²⁶M.K. Singh, R.S. Katiyar and J.F. Scott, *J. Phys.: Condens. Matter* **20** 252203 (2008).
- ²⁷J.F. Scott, M.K. Singh and R.S. Katiyar, *J. Phys.: Condens. Matter* **20** 322203 (2008).
- ²⁸J.F. Scott, M.K. Singh and R.S. Katiyar, *J. Phys.: Condens. Matter* **20** 425223 (2008).
- ²⁹M. Cazayous, Y. Gallais and A. Sakuto, *Phys. Rev. Lett.* **101**, 037601 (2008).
- ³⁰P. Rovillain, M. Cazayous, Y. Gallais, and A. Sacuto, *Phys. Rev.B* **79**, 180411(R) (2009).
- ³¹R. Jarrier, X. Matri, J. H. Albillos, P. Ferrer, R. Houmont, P. Gemeiner, G. Geneste, P. Berthet, T. Schulli, P. Cevc, R. Blink, S. S. Wong, T. J. Park, M. Alexe, M. A. Caepenter, J.F. Scott, G. Catalan and B. Dkhil, *Phys. Rev.B* **85**, 184104 (2012).
- ³²K. Binder and A. P. Young, *Rev. Mod. Phys.* **58**, 4 (1986).
- ³³S. Kamba, D. Nuzhnyy, M. Savinov, J. Šebek, and J. Petzelt, *Phys. Rev. B* **75**, 024403 (2007).
- ³⁴S. O. Leontsev and R. E. Eitel, *J. Am. Ceram. Soc.* **92** 2957-2961 (2009).
- ³⁵J. Rodriguez-Carvajal Laboratory, FULLPROF, a Rietveld and pattern matching and analysis programs version2010, Laboratoire Leon Brillouin, CEA-CNRS, France [<http://www.ill.eu/sites/fullprof/>].
- ³⁶R. Haumont, I. A. Kornev, S. Lisenkov, L. Bellaiche, J. Kreisel and B. Dkhil, *Phys. Rev. B* **78**, 134108 (2008).
- ³⁷R. Palai, R. S. Katiyar, H. Schmid, P. Tissot, S. J. Clark, J. Robertson, S. T. A. Redfern, G. Catalan, and J. F. Scott, *Phys. Rev. B* **78**, 134108 (2008).
- ³⁸S. M. Selbach, M. –A. Einarsrud, and T. Grande, *Chem. Mater.* **21**, 169-173 (2009).
- ³⁹N. Koshizuka and S. Ushioda, *Phys.Rev.B* **22**, 5394 (1980).
- ⁴⁰Y. G. Chukalkin and B.N. Goshchitskii, *Phys. Status Solidi A* **200**, R9 (2003).
- ⁴¹S. Bhattacharya, A. Senyshyn, H. Fuess, and D. Pandey, *Phys.Rev.B* **87**, 054417 (2013).
- ⁴²H. Wu, Y. B. Lin, J. J. Gong, F. Zhang, M. Zeng, M. H. Qin, Z. Zhang, Q. Ru, Z. W. Liu, X. S. Gao, and J. M. Liu, *J. Phys. D: Appl. Phys.* **46** 145001 (2013).
- ⁴³Q. Wang, Q. Sun, G. Chen, Y. Kawazoe, and P. Jena, *Phys.Rev.B* **77**, 205411 (2008).
- ⁴⁴C. E. R. Torres, G. A. Pasquevich, P. M. Zélis, F. Golmar, S. P. Heluani, S. K. Nayak, W. A. Adeagbo, W. Hergert, M. Hoffmann, A. Ernst, P. Esquinazi, and S. J. Stewart *Phys. Rev.B* **89**, 104411 (2014).
- ⁴⁵J. L. Tholence, *Solid State Commun.* **35**, 113 (1980).
- ⁴⁶P. Berge, P. Calmetter, C. Laj, M. Tournarie, and B. Volochine, *Phys. Rev. Lett.* **24**, 1223(1970).
- ⁴⁷A. Singh, V. Pandey, R. K. Kotnala, and D. Pandey, *Phys. Rev. Lett.* **101**, 247602 (2008).
- ⁴⁸Q. Xu, S. Zhou, D. Wu, M. Uhlarz, Y. K. Tang, K. Potzger, M. X. Xu, and H. Schmidt, *J. Appl. Phys.* **107**, 093920 (2010).

- ⁴⁹Y. Yoneda, Y. Kitanaka, Y. Noguchi, and M. Miyayama, *Phys. Rev. B* **86**, 184112 (2012).
- ⁵⁰T. Kawae, Y. Terauchi, H. Tsuda, M. Kumeda, and A. Morimoto, *Appl. Phys. Lett.* **94**, 112904 (2009).
- ⁵¹V. R. Palkar, D. C. Kundaliya, and S. K. Malik, *J. Appl. Phys.* **93**, 4337 (2003).
- ⁵²G. S. Arya and N. S. Negi, *J. Phys. D: Appl. Phys.* **46** 095004 (2013).
- ⁵³M. Kumar, and K. L. Yadav, *Appl. Phys. Lett.* **91**, 242901 (2007).
- ⁵⁴J. Wang, A. Scholl, H. Zheng, S. B. Ogale, D. Viehland, D. G. Schlom, N. A. Spaldin, K. M. Rabe, M. Wuttig, L. Mohaddes, J. Neaton, U. Wagmare, T. Zhao, R. Ramesh, W. Eerenstein, F. D. Morrison, J. Dho, M. G. Blamire, J. F. Scott, and N. D. Mathur, *Science*, **307**, 1203 (2005).
- ⁵⁵C. Ederer and N. A. Spaldin, *Phys.Rev.B* **71**, 224103 (2005).
- ⁵⁶T. R. Paudel, S. S. Jaswal, and E. Y. Tsymbal, *Phys.Rev.B* **85**, 104409 (2012).
- ⁵⁷I. Sosnowska, T. P. Neumaier and E. Steichele, *J. Phys. C: Solid State Phys.* **15**, 4835 (1982).
- ⁵⁸P. Fischer, M. Połomska, I. Sosnowska and M. Szymański, *J. Phys. C: Solid State Phys.* **13** 1931 (1980).
- ⁵⁹R. Przenioslo, A. Palewicz, M. Regulski, I. Sosnowska, R. M. Ibberson, and K. S. Knight, *J. Phys.: Condens. Matter*, **18** 2069-75 (2006).
- ⁶⁰J. H. Albillos, G. Catalan, J. A. R. Velamazan, M. Viret, D. Colson, and J. F. Scott *J. Phys.: Condens. Matter*, **22** 256001 (2010).
- ⁶¹A. Palewicz, I. Sosnowska, R. Przenioslo, and A. W. Hewat, *Acta Physica Polonica A*, **117** 296 (2010).
- ⁶²M. Gabay and G. Toulouse, *Phys. Rev. Lett.* **47**, 201 (1981).
- ⁶³J. Lauer and W. Keune, *Phys. Rev. Lett.*, **48**, 1850 (1982).
- ⁶⁴D. H. Ryan, “*Recent Progress in Random Magnets*”, *World Scientific*, Singapore, (1992).
- ⁶⁵S. Chillal, M. Thede, F. J. Litterst, S. N. Gvasaliya, T. A. Shaplygina, S. G. Lushnikov, and A. Zheludev, *Phys. Rev. B* **87**, 220403(R) (2013).
- ⁶⁶W. Kleemann, V.V. Shvartsman, and P. Borisov, *Phys. Rev. Lett.* **105**, 257202 (2010).

TABLE I. Comparison of fitting parameters including goodness of fit (GoF) for the two models for pure and 0.3 wt% MnO₂ doped BiFeO₃.

Parameters	Vogel-Fulcher Law		Parameters	Scaling Law	
	Pure BiFeO ₃	Doped BiFeO ₃		Pure BiFeO ₃	Doped BiFeO ₃
T _{VF}	21.61 K	20.07 K	$z\nu$	1.862	1.582
E _{act}	0.822 meV	0.849 meV	T _{SG}	21.61 K	20.07 K
τ_0	6.515 x 10 ⁻⁵ s	9.959 x 10 ⁻⁵ s	τ_0	2.975 x 10 ⁻⁵ s	7.922 x 10 ⁻⁵ s
GoF	0.99877	0.99912	GoF	0.99455	0.99576

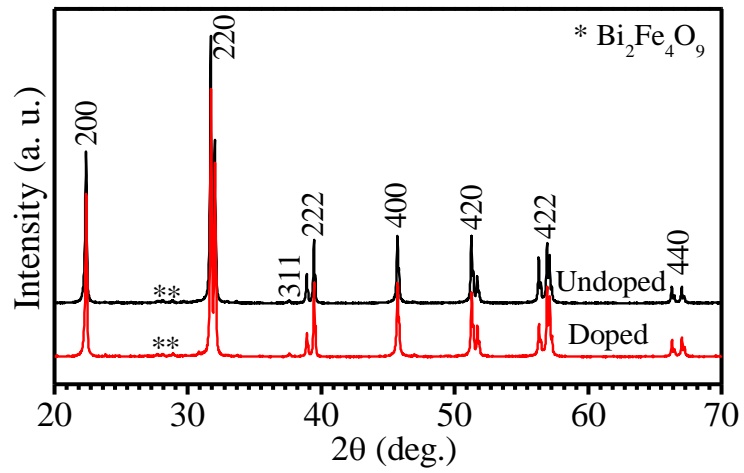


FIG. 1. X-ray diffraction patterns of pure BiFeO_3 and 0.3 wt% MnO_2 doped BiFeO_3 collected at room temperature. All indices are with respect to a doubled pseudocubic cell. The asterisk (*) marks the impurity peak of $\text{Bi}_2\text{Fe}_4\text{O}_9$.

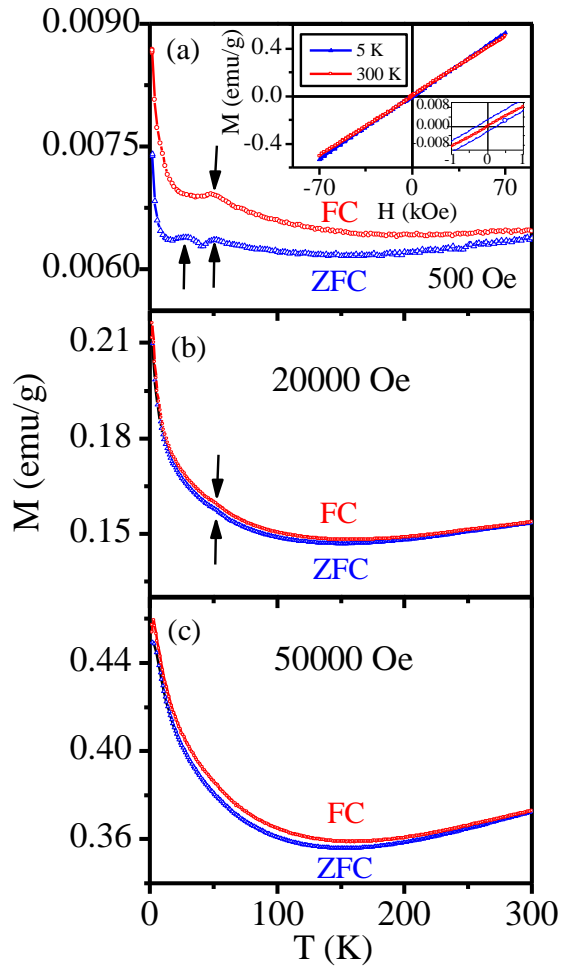


FIG. 2. Temperature dependence of dc magnetization (M) at an applied dc field of (a) 500 Oe (b) 20000 Oe and (c) 50000 Oe for pure BiFeO_3 . Insets to figure depict the M - H plots at 5 K and 300 K.

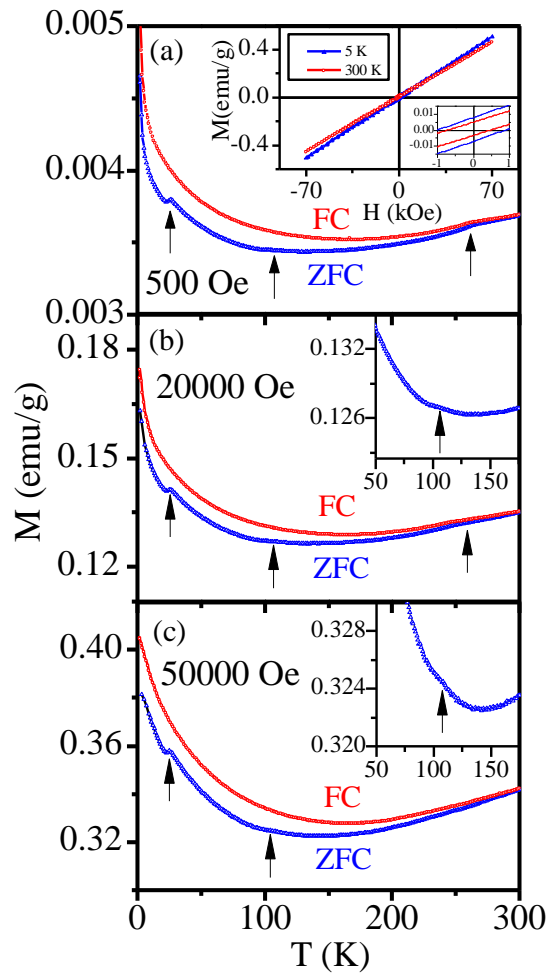


FIG. 3. Temperature dependence of dc magnetization (M) at an applied dc field of (a) 500 Oe (b) 20000 Oe and (c) 50000 Oe for 0.3 wt% MnO_2 doped BiFeO_3 . Insets to figure depict the M - H plots at 5 K and 300 K.

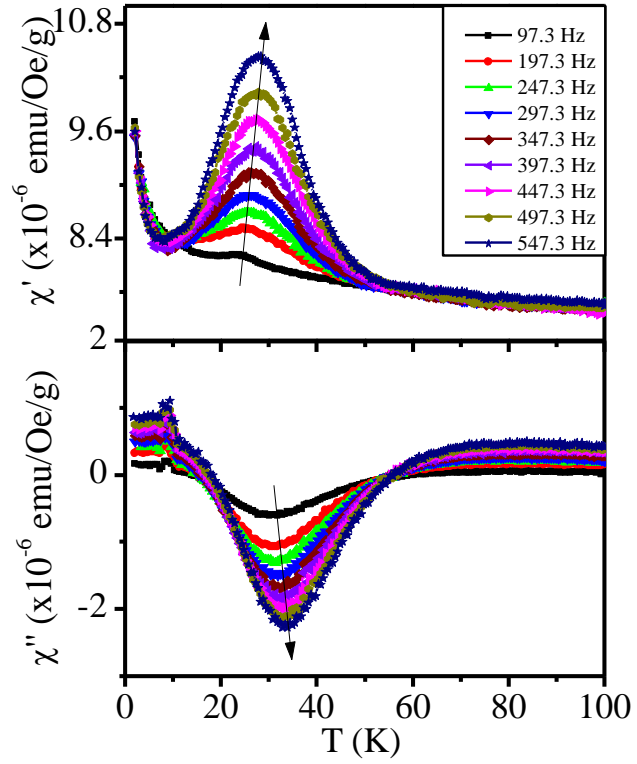


FIG. 4. Temperature dependence of the real and imaginary parts of the ac susceptibility at various frequencies at an applied ac field of 5 Oe for pure BiFeO₃.

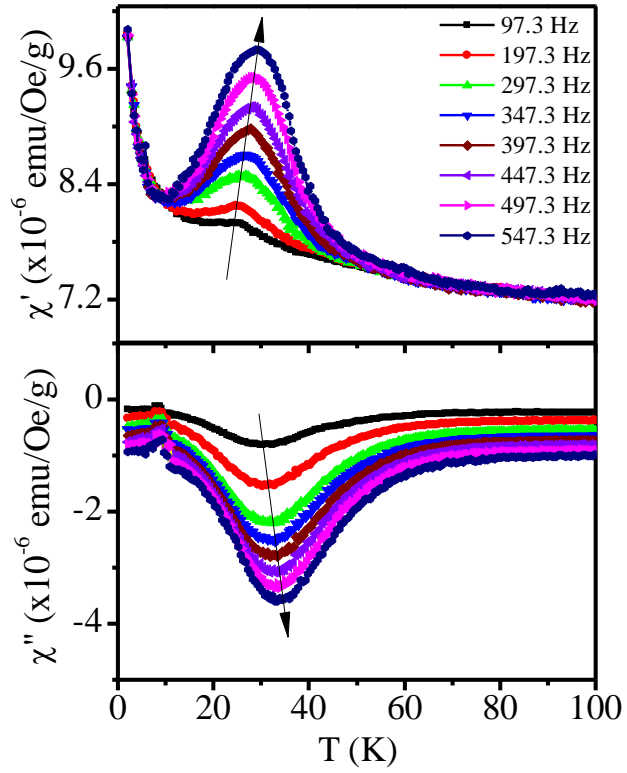


FIG. 5. Temperature dependence of the real and imaginary parts of the ac susceptibility at various frequencies at an applied ac field of 5 Oe for 0.3 wt% MnO_2 doped BiFeO_3 .

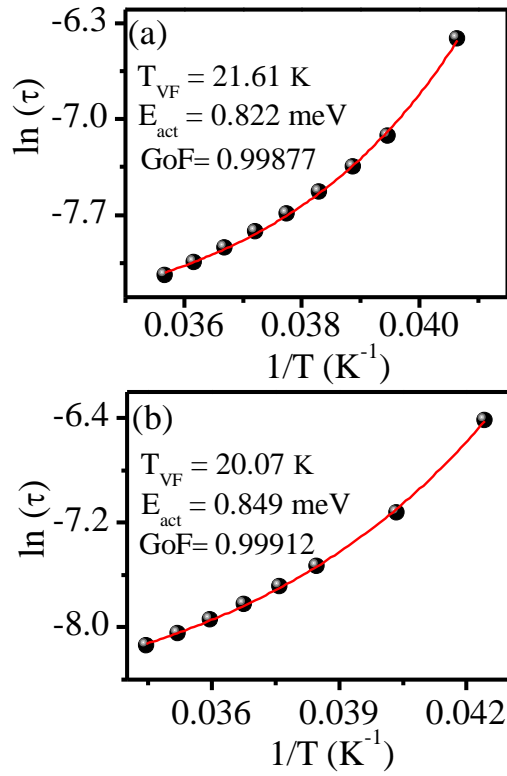


FIG. 6. $\ln \tau$ vs $1/T$ plot. The solid line is the fit for the Vogel-Fulcher law for (a) pure BiFeO_3 and (b) 0.3 wt% MnO_2 doped BiFeO_3 .

Supplementary File

1. Composition analysis:

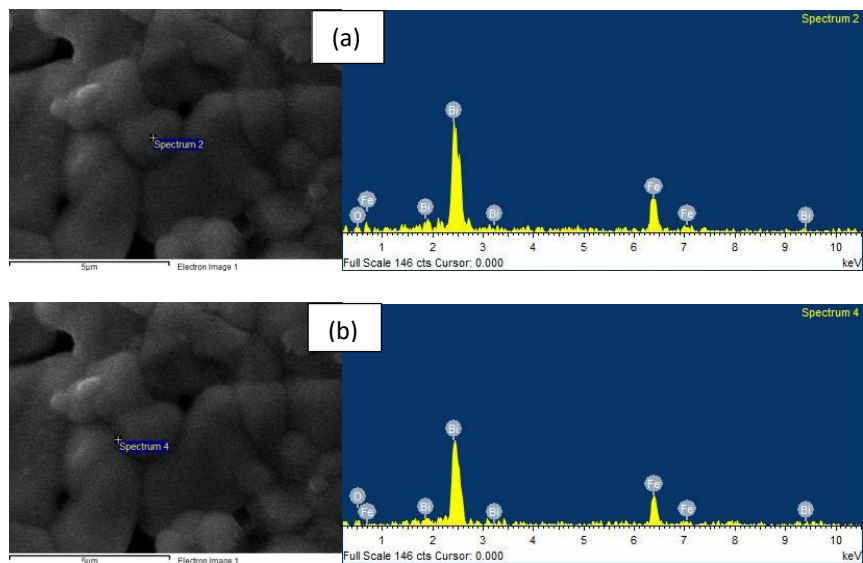


Fig. S1. Microstructure and EDX spectra of BiFeO₃ (a) in the grain and (b) at the grain boundary

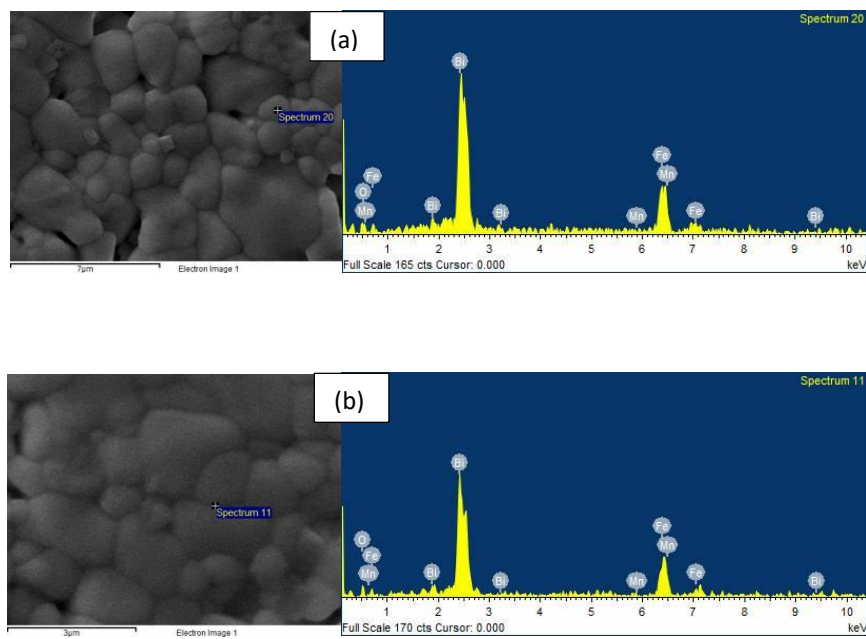


Fig. S2. Microstructure and EDX spectra of 0.3% MnO₂ doped BiFeO₃ (a) in the grain and (b) at the grain boundary.

Table S1: Results of EDX analysis of pure BiFeO₃ and 0.3wt % MnO₂ doped BiFeO₃ in weight percent for the microstructure and spectra shown in Fig. S1 and S2.

Pure BiFeO ₃			0.3wt% MnO ₂ doped BiFeO ₃		
Element	Weight %		Element	Weight %	
	Grain	Grain Boundary		Grain	Grain Boundary
O	11.90	11.28	O	12.54	14.54
Fe	18.74	18.75	Mn	0.33	0.34
Bi	69.36	69.97	Fe	17.58	18.50
			Bi	69.54	66.62
Total	100.00	100.00	Total	100.00	100.00

Table S2: Average composition of the pure BiFeO₃ and 0.3wt % MnO₂ doped BiFeO₃ samples in weight percent.

Pure BiFeO ₃			0.3wt% MnO ₂ doped BiFeO ₃		
Element	Weight%		Element	Weight %	
	Expected	Average		Expected	Average
O	15.3	13.0 ± 1.7	O	15.3	13.6 ± 1.4
Fe	17.9	18.6 ± 0.3	Mn	0.30	0.3 ± 0.1
Bi	66.8	68.4 ± 1.5	Fe	17.9	17.8 ± 0.7
			Bi	66.8	68.3 ± 1.3
Total	100.00	100.00	Total	100.00	100.00

2. LeBail refinement:

The LeBail refinement using R3c space group of BiFeO₃ [7] was carried out for both the samples using FULLPROF package [35]. The observed (filled-circles) and calculated (continuous line) profiles show excellent fit for both the samples, as can be seen from the difference (bottom line) profile given in Fig. S3. This confirms that both the samples belong to the R3c space group. The refined unit cell parameters are listed in Table S3.

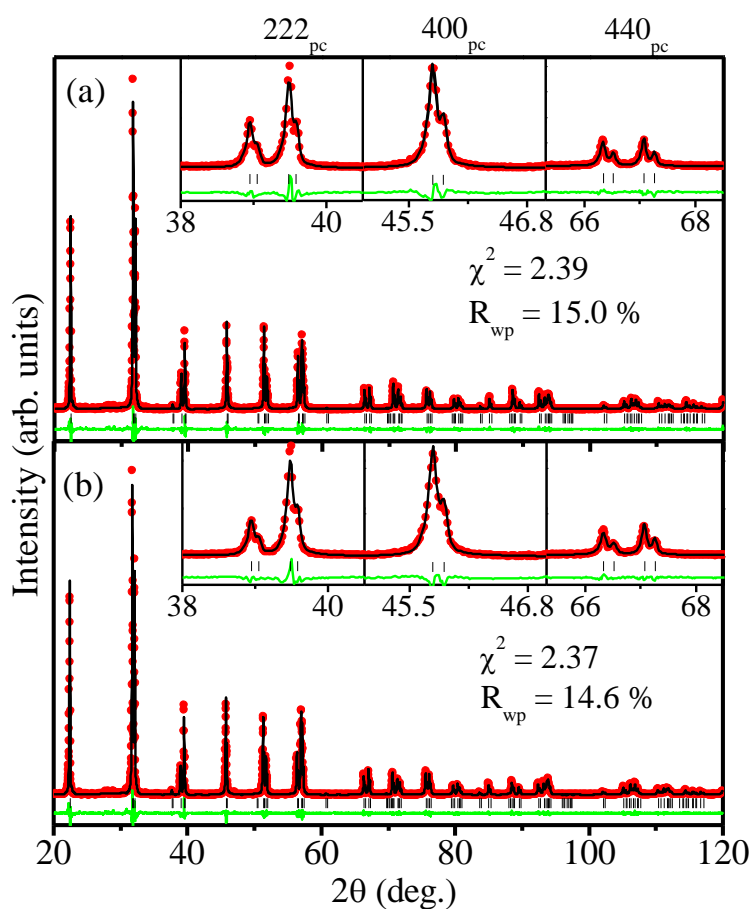


Fig. S3. Observed (filled circles), calculated (continuous line), and difference (bottom line) profiles obtained from LeBail refinement at room temperature using R3c space group for (a) pure BiFeO₃ and (b) 0.3 wt% MnO₂ doped BiFeO₃.

Table S3: LeBail refined unit cell parameters for pure BiFeO₃ and 0.3 wt% MnO₂ doped BiFeO₃ at room temperature.

Parameters	Pure BiFeO ₃	0.3 wt% MnO ₂ doped BiFeO ₃
Space group	R3c	
	Hexagonal unit cell parameters $a = b \neq c, \alpha = \beta = 90^\circ, \gamma = 120^\circ$	
a (Å)	5.5772 (6)	5.5775 (7)
c (Å)	13.8648 (1)	13.8653 (2)
V (Å ³)	373.501 (8)	373.552 (9)
R_{wp} (%)	15.0	14.6
χ^2	2.39	2.37

3. Spin glass dynamics using power law:

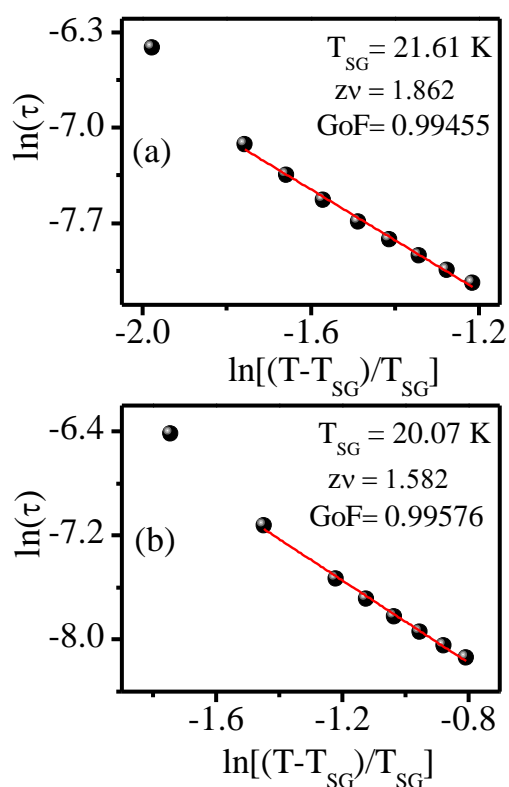


Fig. S4. $\ln\tau$ vs $\ln(T-T_{SG}/T_{SG})$ plot. The solid line is the fit for the power law for (a) pure BiFeO₃ (b) 0.3 wt% MnO₂ doped BiFeO₃.